PNAS
www.pnas.org

Supplementary Information for

Liquid-crystalline phase transitions in lipid droplets are related to cellular states and specific organelle association

Julia Mahamid, Dimitry Tegunov, Andreas Maiser, Jan Arnold, Heinrich Leonhardt, Jürgen M. Plitzko and Wolfgang Baumeister

Corresponding authors: Julia Mahamid, Wolfgang Baumeister
Email: julia.mahamid@embl.de, baumeist@biochem.mpg.de

This PDF file includes:

Materials and Methods
Figs. S1 to S3
Captions for movies S1 to S4
References for SI reference citations

Other supplementary materials for this manuscript include the following:

Movies S1 to S4

www.pnas.org/cgi/doi/10.1073/pnas.1903642116

Materials and methods

Cell culture, treatment and specimen vitrification

Wild type HeLa Kyoto cells, cells expressing mCherry tagged histone off a plasmid constructs (H2B-mCherry), or double tagged line expressing both green fluorescent protein (GFP)-tagged β-tubulin off a bacterial artificial chromosome (BAC) and H2B-mCherry, were cultured at 37°C with 5% CO_2 in Dulbecco's modified Eagle's medium (DMEM; ThermoFischer Scientific, Schwerte, Germany) supplemented with 10% (v/v) fetal bovine serum (FBS), 2 mM L-glutamine, 100 mg/mL penicillin, 100 mg/mL streptomycin and 0.5 mg/mL geneticin (G418) for the BAC-tagged lines.

For measurement on interphase cells, cells were cultivated on Gold Quantifoil grids (R2/2 or R2/1, Au 200 mesh grid, Quantifoil Micro Tools, Jena, Germany). Additional carbon (20–25 nm) was deposited on the film side of the grids in a carbon evaporator (MED 020, BAL-TEC) and plasma cleaned for 45 s prior to their use. Grids were sterilized under UV irradiation in a laminar flow hood for 30 min and immersed in culture medium in a CO_2 incubator for 30 min. Cells were detached from cell culture flasks using 0.05% trypsin-EDTA and seeded on 4-6 pre-treated Quantifoil grids in 35-mm dishes. Cells were kept in an incubator overnight to allow adhesion. Starvation was induced by exchange of the medium to Earle's Balanced Salt Solution (EBSS, ThermoFischer Scientific, Schwerte, Germany) for 5-8 h in the absence or presence of 100 nM Bafilomycine A1 (Sigma-Aldrich Chemie, Munich, Germany) to inhibit autophagosome-lysosome fusion (1). Heat shock was induced by incubation at 43°C for 30 min. Arsenite treatment to disrupt mitochondrial respiration was induced by 1mM $NaAsO_2$ in DMEM media for 30-90 min. For the preparation of synchronized mitotically arrested HeLa cells, cells grown to 80% confluency in a culture flask were treated with 2 mM thymidine for 16 h (S-phase block) and released into a fresh medium for 4-6 h. Mitotic arrest (M-phase block) was achieved by inhibiting the microtubule motor, Eg5, with the small molecule of S-trityl-L-cysteine (STLC; Sigma-Aldrich Chemie, Munich, Germany) (2) 6-8 h before the vitrification at a concentration of 2 μM. Mitotically arrested cells were detached from the culture flask by mechanical shake-off, thus increasing the fraction of the synchronized cells in the suspension as mitotic cells become loosely attached to the substrate upon rounding. The collected suspension was centrifuged at 300 g for 2 min to concentrate the cell pellet. BODIPY fluorescent dyes for labeling of lipid droplets were added to the cell suspension and incubated for 5 minutes at 37°C prior to vitrification (Life Technologies: BODIPY 493/503 – green fluorescence, general neutral lipid stain, final concentration 1 μM; BODIPY 558/568 C12 – red fluorescence, specific to

neutral fatty acids, final concentration 1 μM) (3). Four microliters of the cell suspension were deposited onto the grids for vitrification.

For correlative microscopy experiments, plasma cleaned for 45 s holey 200 mesh copper R 2/1 grids (Quantifoil Micro Tools, Jena, Germany) were pre-incubated with 2 µl of a mixture of 1 µm Dynabeads (Life Technologies, MyOne with 40% iron oxide, carboxylic acid) diluted 1:10 from original stock and 200 nm Tetraspeck (Life Technologies) diluted 1:100 (4).

Grids were blotted from the reverse side with the aid of a Teflon sheet from the front side and immediately plunged into a liquid ethane/propane mixture at liquid nitrogen temperature using a Vitrobot Mark 4 (FEI Company, Eindhoven, Netherlands). The Vitrobot was set to 37°C, 90% humidity, blot force 10, blot time of 10 s and 2 s drain time. The frozen grids were stored in sealed boxes in liquid nitrogen until further processing.

Fluorescent light microscopy and quantification of LDs

Cells were cultured on 80% ethanol cleaned and UV sterilized precision 18 x 18mm #1.5 coverslips. Cell were incubated overnight to allow adhesion and then treated as described above for synchronization, starvation and heat shock. At the end of treatment, cells were fixed with 2% Formaldehyde for 10 min at room temperature, exchanged into 0.02% Tween in PBS and kept overnight at 4°C. Specimens were then washed with 0.5% Triton X-100 in PBS, blocked for 1 h with BSA, and incubated with BODIPY 493/503 at a final concentration of 2 μM for 60 min followed by DAPI for preparations of WT HeLa. Cells were mounted in Vectashied mounting medium and sealed on a glass slide. Stacks were acquired on a wide-field DeltaVision microscope (GE Healthcare) using a 60x oil immersion objective. Following deconvolution, images were processed in ImageJ for signal normalization, segmentation of individual cells, and quantification of LD number, size and total volume/cell using the 3D object counter plugin (5). Quantification is presented as LD volume/cell to account for the observed change in both LD number and size by light microscopy using BODIPY. BODIPY/cell is represented here as a fold increase relative to the control cells. Six cells were analyzed per condition.

Cryo-FIB

Cryo-FIB lamella preparation was performed as described in (6). Plunge frozen grids fixed into autogrids modified for FIB preparation were mounted into a shuttle (7). The shuttle was transferred into a dual-beam (focused ion beam(FIB)/scanning electron microscope(SEM)) microscope (Quanta

3D FEG, FEI, the Netherlands) using a cryo-transfer system (PP3000T, Quorum Technologies, Laughton, Lewes, East Sussex, Great Britain). During FIB operation, samples were kept at constant liquid nitrogen temperature using an in-house developed open nitrogen-circuit 360° rotatable cryo-stage (8). To improve sample conductivity and reduce curtaining artifacts during FIB milling, the samples were first sputter-coated with platinum in the Quorum prep-chamber (10 mA, 30 s) and then coated with organometallic platinum using the *in situ* gas injection system (GIS, FEI) operated at room temperature, 12 mm stage working distance and 5 s gas injection time. Lamellae were prepared using Gallium ion beam at 30 kV at stage tilt angles of 15°-20°. Lamella preparation is conducted in a stepwise rough milling with high currents of 0.5 nA, gradually reduced to lower currents, down to 50 pA for the final cleaning steps. Progress of the milling process was monitored using the scanning electron beam operated at 10 kV and 42 pA. For improved conductivity of the final lamella for specimens intended for phase plate tomography, we again sputter coated the grid after cryo-FIB preparation with platinum in the Quorum prep-chamber (10 mA, 1 s). The thickness of the platinum layer was determined from the tomographic reconstructions to be < 5 nm.

3D correlation

3D correlation was performed essentially as described in (4). Briefly, frozen grids were clipped into autogrid specimen cartridges modified for FIB preparation under shallow angles (7) and imaged by light microscopy using the FEI CorrSight microscope (FEI, Eindhoven, the Netherlands) equipped with a CorrSight Cryo-Module at liquid nitrogen temperature. Data acquisition used for the correlation was done with a Zeiss EC Plan-Neofluar 40x/0.9 NA Pol (WD = 410 µm) air objective, a spinning disk confocal equipped with a laser light source through an FEI spinning disk confocal setup, and a 1344 x 1024 pixel camera with a pixel size of 6.4 µm (Hamamatsu Digital Camera C10600 ORCA-R2). The combination of the camera's physical pixel size with the 40x objective resulted in an image pixel size of 161.25 nm. The resolution of the system was determined with point-spread-function (PSF) measurements on 200 nm diameter fluorescent beads. For the green fluorescence channel (λ= 488 nm), the determined resolution is: x = 580 nm; y = 570 nm; z = 2 µm (parallel to the optical path). The PSF is practically identical for all channels because the performance is limited by the wavelength-independent optical settings of our system rather than by the Abbe diffraction limit.

Image acquisition was done with the FEI MAPS 2.1 software operated in semi-automated mode to generate montages of the grids and for the acquisition of spinning disk confocal stacks at multiple

areas of interest. The frozen grids were stored in sealed boxes in liquid nitrogen until further processing. Once transferred into the dual-beam (FIB/SEM) microscope (described above), the areas of interest, as judged from the cryo-FLM data, were visually identified and both an SEM image and FIB image of the area containing all fiducials needed for correlation were acquired. 3D coordinate transformation was performed based on beads that are clearly distinguishable in the FLM and SEM/FIB data, as implemented in the graphical user interface of the 3D Correlation toolbox (3DCT; https://3dct.semper.space/). The accuracy of the correlation depends on the precision in fitting the centres of mass of the markers, detected by a gaussian fit of the intensity in 3 dimensions in the fluorescence data. A spherical marker shape is advantageous for a precise determination of its centre. Beads of 1 µm diameter were used because these were the smallest that were reliably detected in SEM/FIB. For coordinate transformation, corresponding fiducials are identified in both the spinning disk confocal fluorescence and SEM/FIB. The FIB view at a typical milling angle (stage tilt of 15°-25°, corresponding to 7°-18° with respect to the grid plane) is equivalent to a side view of the FLM volume, corresponds to a viewing angle of 7°-18° with low axial resolution. Errors in fitting of the fluorescence signal in the z-direction therefore translate to errors along the y-axis in the FIB image.

The accuracy of the coordinate transformation was previously evaluated by the 'leave-one-out' cross validation test on bead-only data. The mean error in x and y (in the FIB image), as a function of the number of markers that were used for the correlation, shows that accuracy in the range of tens of nanometres can be achieved with a minimum of 4 markers. For cellular specimens, a larger number of fiducials (8-16) is typically used to ensure higher correlation accuracy, which then reaches the sub-pixel range (<160 nm). To clarify, high-accuracy in the correlation calculation does not necessarily produce precisely targeted lamellae, due to technical limitations during the FIB milling process (stage and image drift). Therefore, a second transformation is calculated after lamella preparation to identify the true lamella position in the original confocal volume: once thin lamellae were produced by FIB milling (described above) following correlation to target agglomerates of LDs and were subsequently observed by cryo-TEM, a second correlation step was performed to navigate acquisition of cryo-TEM data at fluorescently labeled positions within the lamella. This required correlation between the original spinning disk confocal fluorescence volume and the TEM montage. To do this, a FIB image of the final lamella (including the fiducials originally used for the correlation) is used to retrieve the actual final lamella position within the original fluorescence volume. The fluorescence volume is deconvolved to reduce the influence of the PSF.

Then a slice through the fluorescence volume is computationally extracted at this position. The slice, typically 2 pixels in thickness corresponding to roughly 300 nm, approximated to fit the lamella thickness, is transformed using calculations based on the fiducials to fit the SEM view of the final lamella. Finally, the TEM montage of the lamella is correlated in 2D to the SEM image of the final lamella based on features at the edges of the lamella. The 2D correlation was produced using the 3-point correlation function in the MAPS software. This allows superimposing the fluorescence oblique slice onto the lamella TEM montage and to identify fluorescently labeled objects within the montage.

Cryo-TEM and tomography

Cryo-electron microscopy data were collected on a Titan Krios microscope operated at 300 kV (FEI) equipped with a field-emission gun, a Quantum post-column energy filter (Gatan, Pleasanton, CA, USA), a K2 Summit direct detector camera (Gatan) and a Volta phase plate (FEI). Data was recorded in dose fractionation counted mode for tomography and super-resolution mode for 2D projections. Tilt-series images were collected using standard automated acquisition procedures with SerialEM software (9). Cryo-EM acquisition parameters were as follows: EFTEM magnification 42000x corresponding to pixel size of 0.342 nm. For 2D projections, the pre-tilt of lamellae with respect to the grid plane due to cryo-FIB milling at shallow angles (10-15°) was corrected for by tilting the stage on the microscope; total dose 10-40 $e^-/Å^2$; 0.5 - 2 μm defocus. For tomography, the tilt range for FIB milled lamellae depended on the pre-tilt of the lamella and is typically ±50° to ±60°; tilt increment 2°; total dose ~ 100 $e^-/Å^2$; 4 μm defocus or target defocus 0 for phase plate tomography; alignment and operation of the Volta phase plate were carried out as described by Fukuda *et al.* (10).

LD spacing measurements in 2D projections

Micrograph movies were aligned and averaged using an in-house implementation of the MotionCor 1 algorithm (11), applied to whole frames. All subsequent analysis was performed in Matlab (Mathworks, 2016), utilizing subroutines from the TOM toolbox (12). The global CTF parameters for each aligned micrograph were estimated, and contrast reversal corrected by phase flipping. Suitable micrographs containing LDs were selected and the global LD positions determined manually. These positions were used to extract individual LDs in square boxes. Leveraging the highly circular LD shape, the image data were remapped from Cartesian to polar coordinates. A synthetic template resembling the side projection of a single CE layer was prepared using a

Gaussian function. The template was cross-correlated with the polar-transformed LD data, sampling a narrow range of rotation angles to account for deviations of the LD shape from a perfect circle. The width of the Gaussian function was optimized to maximize the normalized cross correlation peaks within the smectic phase. Correlation ridges belonging to one CE layer were traced by picking a correlation peak belonging to the outer-most layer, and walking along adjacent peaks in the angular dimensions, while allowing for minor deviations in the radial dimension to account for shape imperfections. Whenever a full layer had been traced, or the correlation was too low to continue tracing, a peak belonging to the next CE layer was searched for along the radial dimension in the inward direction, and the layer traced from there. In case the previous layer contained low-correlation gaps, the next layer was used as a starting point for searches along the radial dimension in the outward direction to trace more parts of the previous layer. This procedure continued until no further CE layers could be added. The traced layers were then used to calculate the spacing statistics over all pairs of closest points on adjacent layers.

A similar tracing procedure was employed for lipid bilayers: Here, the complex bilayer shapes were traced manually in ImageJ (13) and a straight, unwarped version of each bilayer was extracted such that the longitudinal dimension corresponded to the angular dimension of polar-transformed LDs. The width of the synthetic template was optimized independently. The tracing algorithm was limited to only two layers.

Processing of tilt-series and segmentation

Tilt series alignment and tomographic reconstructions were performed using the IMOD software package, version 4.5.7 (http://bio3d.colorado.edu/imod/) (9). In absence of fiducial gold nanoparticles in the FIB-lamellas, alignment of tilt-series projection images was performed with patch-tracking. Final alignment of the tilt-series images was performed using the linear interpolation option in IMOD without CTF correction. For tomographic reconstruction, the radial filter options were left at their default values (cut off, 0.35; fall off, 0.05). Segmentation of membranes and LDs was performed using the tensor voting procedure (14) implemented in Matlab and manually refined in Amira (FEI Visualization Sciences Group). Final annotated images were rendered with the UCSF Chimera package (http://www.cgl.ucsf.edu/chimera).

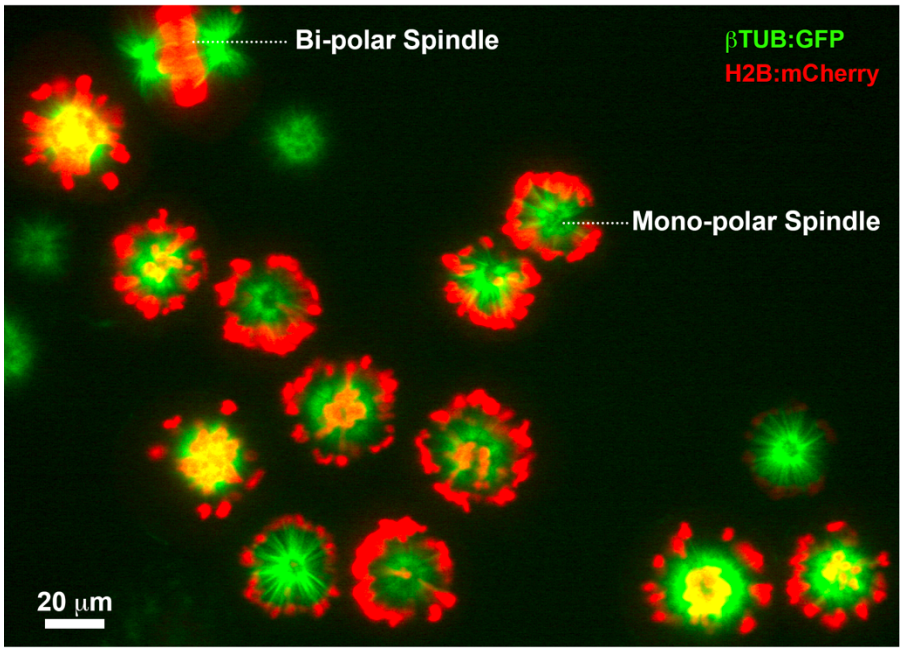

Fig. S1. Internal organization of mono-polar spindles in STLC mitotically arrested HeLa cells. Maximum intensity projection of live-cell spinning disk confocal stack shows that most cells exhibit a radial array of microtubules (green: βTUB:GFP) with condensed chromosomes (red: H2B:mCherry) organized around this spindle.

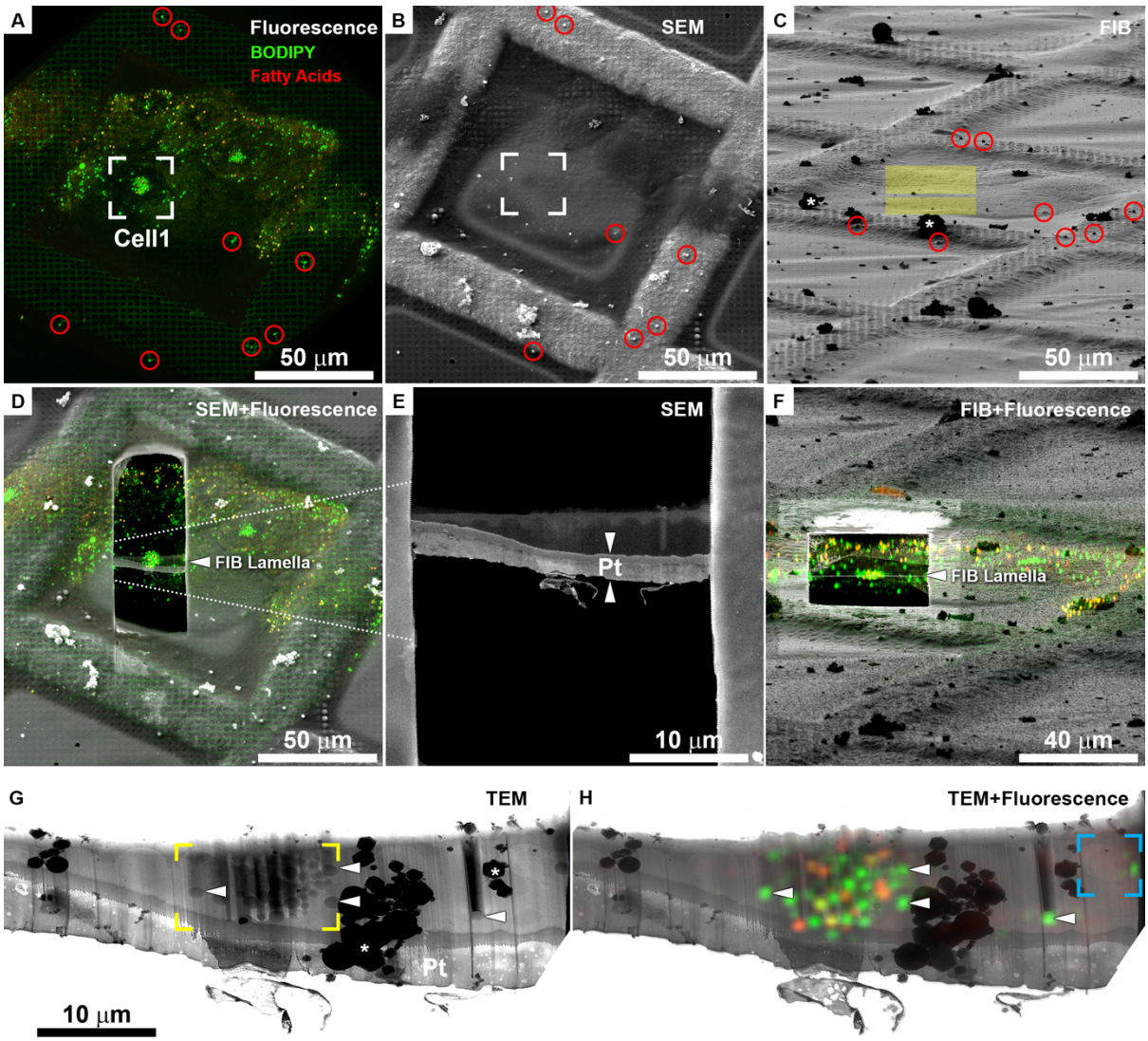

Fig. S2. 3D cryo-correlative light and electron microscopy applied to synchronized, mitotically arrested, HeLa cell culture for targeting fluorescently labelled lipid droplets. A. Maximum intensity projection of a spinning disk confocal volume of frozen-hydrated cells. Green: general neutral lipid dye (BODIPY) and magnetic beads used as fiducials (red circles; levels were adjusted separately inside encircled areas for better visualization of the fiducials). Red: neutral fatty acids dye. Cell 1 delineated by white frame was targeted for cryo-FIB lamella preparation. **B.** SEM and **C.** FIB image at the same sample position; yellow rectangles indicate milling patterns within which material is site-specifically ablated in the FIB thinning process. 3D correlation was performed with the encircled 8 beads in A-C. * in C denote ice crystals introduced during transfer to the FIB/SEM. **D.** SEM top view of the final lamella produced by FIB milling overlaid with FLM data after applying

coordinate transformation. **E**. higher magnification SEM image showing the final lamella. Pt denotes the layer of protective organometallic platinum applied prior to milling. **F**. FIB side view overlaid with FLM data after applying coordinate transformation. Large agglomeration of LDs is retained in lamella. **G**. cryo-TEM montage of lamella. Lamella orientation as in D-F. Arrowheads indicate some of the dense LDs. * denote ice crystals introduced during transfer to the TEM. Area in yellow frame is enlarged in Figure 1.A. **H**. Overlay of cryo-TEM montage of lamella with a computer-generated oblique slice through the confocal volume. LDs stained in green or red are distinguishable within the lamella and colocalize with round dense particles. Area in blue frame is enlarged in Figure 1.D.

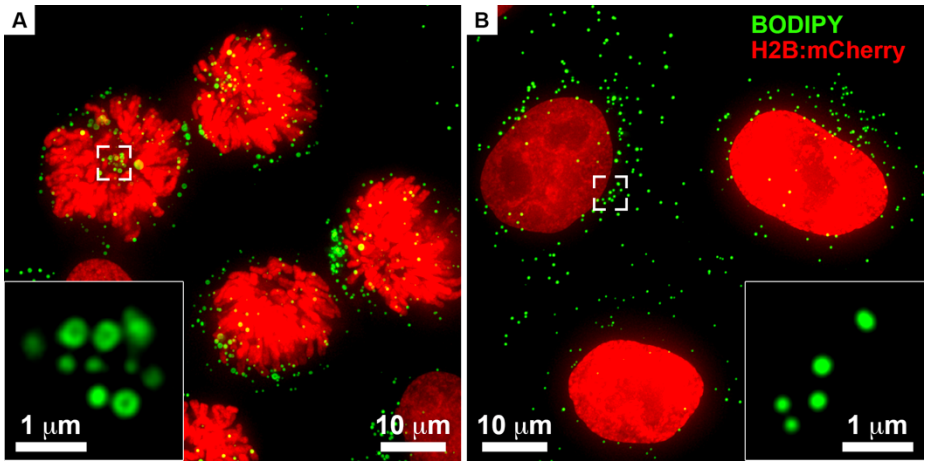

Fig. S3. LD quantification by light microscopy using BODIPY 493/503 in a HeLa H2B:mCherry line. The human histone H2B gene is fused to the gene encoding mCherry to monitor cell cycle phases. **A, B.** Maximum intensity projections of mitotically arrested (A) and control cells (B). Insets: enlarged views of a single optical slice of framed areas in A and B.

Movie S1: BODIPY 493/503 (green) staining in mitotically arrested HeLa H2B:mCherry (red) cell line recapitulates the shell-core organization of LDs. Focal slices through a deconvolved wide-field fluorescence light microscopy stack.

Movie S2. Tomographic volume of a mitotically arrested HeLa cell related to Fig. 3 A & B. Scale bare: 100 nm.

Movie S3. Tomographic volume of a mitotically arrested HeLa cell related to Fig. 3 D. Scale bare: 100 nm.

Movie S4. Tomographic volume of a starved HeLa cell related to Fig. 3 E. Scale bare: 100 nm.

References

1. Yamamoto A, et al. (1998) Bafilomycin A1 prevents maturation of autophagic vacuoles by inhibiting fusion between autophagosomes and lysosomes in rat hepatoma cell line, H-4-II-E cells. Cell Struct Funct 23(1):33-42.
2. Skoufias DA, et al. (2006) S-trityl-L-cysteine is a reversible, tight binding inhibitor of the human kinesin Eg5 that specifically blocks mitotic progression. Journal of Biological Chemistry 281(26):17559 –17569.
3. Rambold AS, Cohen S, & Lippincott-Schwartz J (2015) Fatty acid trafficking in starved cells: regulation by lipid droplet lipolysis, autophagy, and mitochondrial fusion dynamics. Dev Cell 32(6):678-692.
4. Arnold J, et al. (2016) Site-Specific Cryo-focused Ion Beam Sample Preparation Guided by 3D Correlative Microscopy. Biophys J 110(4):860-869.
5. Bolte S & Cordelieres FP (2006) A guided tour into subcellular colocalization analysis in light microscopy. J Microsc-Oxford 224:213-232.
6. Schaffer M, et al. (2017) Optimized cryo-focused ion beam sample preparation aimed at in situ structural studies of membrane proteins. J Struct Biol 197(2):73-82.
7. Rigort A, et al. (2010) Micromachining tools and correlative approaches for cellular cryo-electron tomography. J Struct Biol 172(2):169-179.
8. Rigort A, et al. (2010) A 360º Rotatable Cryo-FIB Stage for Micromachining Frozen-Hydrated Specimens for Cryo-Electron Tomography. Microscopy and Microanalysis 16(Suppl. 2):pp 220-221.

9. Kremer JR, Mastronarde DN, & McIntosh JR (1996) Computer Visualization of Three-Dimensional Image Data Using IMOD. J Struct Biol 116(1):71-76.
10. Fukuda Y, Laugks U, Lucic V, Baumeister W, & Danev R (2015) Electron cryotomography of vitrified cells with a Volta phase plate. J Struct Biol 190(2):143-154.
11. Li X, et al. (2013) Electron counting and beam-induced motion correction enable near-atomic-resolution single-particle cryo-EM. Nature methods 10(6):584-590.
12. Nickell S, et al. (2005) TOM software toolbox: acquisition and analysis for electron tomography. J Struct Biol 149(3):227-234.
13. Schneider CA, Rasband WS, & Eliceiri KW (2012) NIH Image to ImageJ: 25 years of image analysis. Nature methods 9(7):671-675.
14. Martinez-Sanchez A, Garcia I, Asano S, Lucic V, & Fernandez JJ (2014) Robust membrane detection based on tensor voting for electron tomography. J Struct Biol 186(1):49-61.